Applied Thermal Engineering 65 (2014) 24–33

Contents lists available at ScienceDirect

Applied Thermal Engineering

journal homepage: www.elsevier.com/locate/apthermeng

A multi-fluid model for non-equilibrium condensation in gaseous carrier flows

Xiaofei Lv, Bofeng Bai*

State Key Laboratory of Multiphase Flow in Power Engineering, Xi'an Jiaotong University, Xi'an 710049, China

HIGHLIGHTS

- A multi-fluid model is developed for condensing flow in the presence of carrier gas.
- Both the inter-phase velocity slip and temperature difference are taken into account.
- Good agreement is observed between CFD and experimental data.
- The effects of the inter-phase slip are remarkable.

ARTICLE INFO

Article history:
Received 13 September 2013
Accepted 24 December 2013
Available online 4 January 2014

Keywords:
Condensation
Multi-fluid model
Carrier gas
Inter-phase slip
Non-equilibrium

ABSTRACT

The inter-phase slip plays an important role in simulating the condensing flow, which is, however, generally neglected in most numerical studies. To address this, a generalized multi-fluid model is newly developed to predict the two-phase condensing flow in the presence of a carrier gas, where both the inter-phase velocity slip and the temperature difference are taken into account. The multi-fluid model is performed to simulate the condensing flow in two types of supersonic nozzles. Also, the traditional no-slip model is employed for comparing with the multi-fluid model. The simulated results obtained from the multi-fluid model are found to agree better with the experimental data. The effects of the inter-phase slip are revealed qualitatively by comparing the results obtained from these two models. The results show that the effects of inter-phase slip should not be neglected in the whole condensation process. At the initial stage of condensation, both the inter-phase velocity slip and temperature difference are noteworthy. When the condensation finishes and the gas–liquid equilibrium achieves, the inter-phase velocity slip and temperature difference become slight and can be neglected.

1. Introduction

Prediction for vapor condensation in gaseous carrier flows is scientifically interesting in various industrial and technological areas [1–4]. It is noted that the presence of carrier gas makes the condensation process much more complex than the wet steam condensation. As one knows, the carrier gas has a potential effect on the equilibrium vapor fugacity and surface tension due to the mutual interactions between the vapor and carrier gas molecules [5], and would affect the nucleation process by being present in the interior of condensing droplets. Generally, such condensation phenomenon is a complex non-equilibrium process in rapidly expanding flow, the characteristics of which strongly depend on the coupling between the flow field and the condensation process itself. In order to accurately predict the two-phase condensing flow, all physical features such as turbulent gas–liquid flow, the effects of carrier gas on condensation, inter-phase heat and mass transfer due to vapor condensation and momentum transfer as a result of inter-phase velocity slip should be accounted for.

The condensing flow has been experimentally [6–11] and numerically [12–17] studied in different fields for centuries. Generally, Eulerian representation is applied for describing the gas phase, while the condensed phase can be modeled by two ways, i.e., Lagrangian particle tracking approach [18–20] and Eulerian schemes [21–23]. And in general, most calculations using above schemes were performed by imposing a no-slip condition between the phases, which is the so-called no-slip model [24]. Actually, the inter-phase slip has a significant effect not only on the accurate prediction of the velocity field but also on the spontaneous condensation process due to the strong inter-phase coupling between the gas and dispersed liquid phases. However, few attempts have been made on the effects of inter-phase slip, which is potentially significant for simulating the condensing flow.

* Corresponding author. Tel./fax: +86 29 82665316.
E-mail address: bfbai@mail.xjtu.edu.cn (B. Bai).

1359-4311/$ – see front matter
http://dx.doi.org/10.1016/j.applthermaleng.2013.12.060

In recent years, only a few studies have been reported to investigate the effects of inter-phase slip on condensing flow. Wu et al. [25] established a two-fluid model for steam condensing flow, taking the velocity slip and the turbulent diffusion into consideration. Gerber et al. [26] developed an Eulerian multiphase model for the prediction of steam condensation in transonic flow. Dykas et al. [24,27] proposed a two-fluid model to predict the wet steam losses in the low-pressure turbine stages and the model was implemented into the in-house CFD code. It should be noted that the above researches mainly focused on the wet steam flow. To the authors' best knowledge, only few published reports took the velocity slip into account for the prediction of condensation in gaseous carrier flows. Jones et al. [28] adopted a multi-phase multi-size group (MUSIG) population balance model to predict droplet size distributions in Laval nozzles. Prast et al. [1]employed the multi-phase mixture model for calculations of multi-component condensation in the Twister separator, and the inter-phase slip was calculated with the Algebraic Slip Model (ASM). However, the effects of velocity slip were still not clarified in the abovementioned work, and it was found difficult to achieve robust convergence for the multi-phase solver [29].

In this paper, we established a tractable multi-fluid model to characterize the vapor condensation in the presence of a carrier gas. In the newly developed model, both the inter-phase velocity slip and temperature difference were taken into account. In order to comprehensively investigate the effects of inter-phase velocity slip, the present model was compared with the no-slip model and performed to simulate the condensing flow in two supersonic nozzles. On the basis of the numerical simulating results, the proposed models were verified carefully with the existing experimental data. Then the effects of the inter-phase slip were qualitatively determined. Finally, the inertial non-equilibrium and thermal non-equilibrium were analyzed in detail to investigate the interactions between the two phases.

2. Mathematical models and numerical implementation

The schematic of condensing system studied in this paper is shown in Fig. 1, which consists of a carrier gas, a condensable vapor and vast amounts of liquid droplets, and the volume fractions of the vapor and droplets are very small. The basic idea of the common multi-fluid model is treating the dispersed phase as pseudo-fluid [30], thus both phases are described as inter-penetrating continua in the gas-droplet two-phase flow. In the newly developed multi-fluid model, the carrier gas and condensable vapor are described as two independent fluids for the condensing system abovementioned, besides treating the liquid droplets as pseudo-fluid. Therefore, the two-phase condensing flow is considered as a three-fluid flow, where each fluid has individual constitutive equations solved in an Eulerian framework. One assumption is made in this paper: the carrier gas, as a non-condensing constituent, is absent in the interior of liquid droplets.

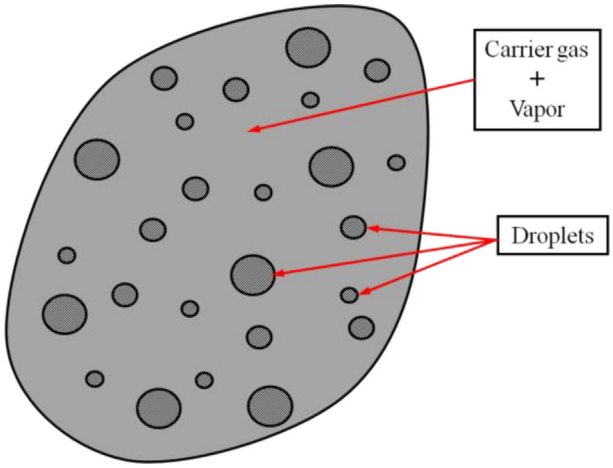

Fig. 1. Schematic of the condensing system.

Since the two gas fluids have the same velocity and temperature, the momentum and energy equations of condensable vapor are unnecessary when the constitutive equations of the carrier gas have been solved. In addition, based on the assumption of no carrier gas existed in the interior of liquid droplets, once the mass conservation equation of liquid phase has been solved, the mass fraction of the condensable vapor can be deduced according to conservation of mass for the whole condensing system, so the continuity equation of vapor can be disregarded. For further simplification, the droplet temperature can be calculated by a high accuracy explicit formula without solving the energy equation of liquid phase. Finally, the multi-fluid model is reduced to the form of separate continuity and momentum equations for carrier gas and liquid droplet phase together with the energy equation for carrier gas. The phase interactions are involved through appropriate source terms of the equations.

As the liquid droplets occupy little volume in the condensing flow and the droplets are sufficiently small (submicron-size and below), it is assumed that the gas phase turbulence remains unaffected by the presence of droplets. However, the gas phase turbulence would affect the dispersion of the droplets. The turbulence effects on the droplet motion are included in the liquid phase equations. Since the methodology of non-equilibrium condensing flow model is independent on the type of turbulence model, the well-established standard $k-\varepsilon$ model is adopted for the condensing flow modeling in present study. For brevity, the equations of the turbulence model are not listed here. Moreover, the no-slip model is depicted in the following section for comparison.

2.1. Multi-fluid model

In the multi-fluid model, both the inter-phase slip and temperature difference are taken into account, so each phase has its own velocity and temperature. Both the gas and liquid phase have individual governing equations, the governing equations for gas phase are as follows:

$$\frac{\partial\left(\rho_g\right)}{\partial t}+\frac{\partial}{\partial x_j}\left(\rho_g u_j\right)=0 \tag{1}$$

$$\frac{\partial\left(\rho_g u_i\right)}{\partial t}+\frac{\partial}{\partial x_j}\left(\rho_g u_j u_i\right)=-\frac{\partial p}{\partial x_i}+\frac{\partial \tau_{ij}}{\partial x_j}-F_{Di} \tag{2}$$

$$\frac{\partial\left(\rho_g E_g\right)}{\partial t}+\frac{\partial}{\partial x_j}\left(u_j\left(\rho_g E_g+p\right)\right)=-\frac{\partial q_j}{\partial x_j}+\frac{\partial\left(u_i\tau_{ij}\right)}{\partial x_j}+\beta\dot{m}h_{fg}-u_i F_{Di} \tag{3}$$

where the subscript g denotes carrier gas, p, ρ_g, u_i, F_{Di}, τ_{ij}, T_g and E_g represent the local pressure, gas density, i-wise velocity component, i-wise drag force component, viscous stress tensor, temperature and total energy, respectively. h_{fg} is the latent heat of vapor, $\dot{m}$ is the mass condensation rate, and β is the proportion of the latent heat absorbed by the carrier gas.

To adequately model the liquid phase behavior, the condensation process is described by the Hill's method [31]. Including the

turbulence effects on the dispersion of the droplets, the governing equations for liquid phase are given by,

$$\frac{\partial\left(\rho_g Q_0\right)}{\partial t}+\frac{\partial}{\partial x_j}\left(\rho_g Q_0 u_{lj}\right)=\frac{\partial}{\partial x_j}\left(\Gamma_t\frac{\partial Q_0}{\partial x_j}\right)+J \tag{4}$$

$$\frac{\partial\left(\rho_g Q_1\right)}{\partial t}+\frac{\partial}{\partial x_j}\left(\rho_g Q_1 u_{lj}\right)=\frac{\partial}{\partial x_j}\left(\Gamma_t\frac{\partial Q_1}{\partial x_j}\right)+Jr_c+\rho_g Q_0\frac{d\bar{r}}{dt} \tag{5}$$

$$\frac{\partial\left(\rho_g Q_2\right)}{\partial t}+\frac{\partial}{\partial x_j}\left(\rho_g Q_2 u_{lj}\right)=\frac{\partial}{\partial x_j}\left(\Gamma_t\frac{\partial Q_2}{\partial x_j}\right)+Jr_c^2+2\rho_g Q_1\frac{d\bar{r}}{dt} \tag{6}$$

$$\frac{\partial\left(\rho_g Y\right)}{\partial t}+\frac{\partial}{\partial x_j}\left(\rho_g Y u_{lj}\right)=\frac{\partial}{\partial x_j}\left(\Gamma_t\frac{\partial Y}{\partial x_j}\right)+\dot{m} \tag{7}$$

$$\begin{aligned}\frac{\partial\left(\rho_g Y u_{li}\right)}{\partial t}+\frac{\partial\left(\rho_g Y u_{lj}u_{li}\right)}{\partial x_j}=&-\frac{\partial\alpha_l p}{\partial x_i}+\frac{\partial}{\partial x_j}\left[\mu_t Y\left(\frac{\partial u_{lj}}{\partial x_i}+\frac{\partial u_{li}}{\partial x_j}\right)\right]\\&+\frac{\partial}{\partial x_j}\left[\Gamma_t\left(u_{lj}\frac{\partial Y}{\partial x_i}+u_{li}\frac{\partial Y}{\partial x_j}\right)\right]+F_{Di}\\&+\dot{m}(u_i-u_{li})\end{aligned} \tag{8}$$

where Q_0, Q_1 and Q_2 represent zeroth, first and second moments of the droplet size distribution, and Q_0 corresponds to the number density of the liquid droplets. Γ_t is the turbulent diffusivity calculated by $\Gamma_t=\mu_t/\sigma_t$. Y is the mass fraction of liquid phase, i.e., wetness. The average droplet radius is approximated by,

$$\bar{r}=\sqrt{\frac{Q_2}{Q_0}} \tag{9}$$

The mass condensation rate is calculated as follows,

$$\dot{m}=\frac{4}{3}\pi\rho_l\left(Jr_c^3+3\rho_g Q_2\frac{d\bar{r}}{dt}\right) \tag{10}$$

where ρ_l, r_c, J and $d\bar{r}/dt$ are liquid density, critical radius, nucleation rate, and droplet growth rate, respectively.

The inter-phase drag force, which is taken account in momentum equations, is the source of inter-phase slip. The generalized drag force formula for the condensing droplets in the entire range of the Knudsen number (which is a dimensionless measure of the relative magnitudes of the gas mean free path and the particle size) is adopted [32],

$$\boldsymbol{F_D}=-\frac{8}{3}\rho_g Q_0\left(1+\alpha'^{-1.143}\right)^{-0.875}\sqrt{2\pi m_r k_B T}Nr^2\Omega_{avg}^{(1,1)^*}\boldsymbol{V} \tag{11}$$

where

$$\alpha'=\frac{9\sqrt{2\pi}\mu}{8\Omega_{avg}^{(1,1)^*}\sqrt{m_r k_B T}Nr} \tag{12}$$

where, k_B is the Boltzmann's constant, $m_r=m_g m_d/(m_g+m_d)$ is the reduced mass, $\boldsymbol{V}$ is the velocity vector of the droplet relative to the gas, N is the number density of the gas.

$\Omega_{avg}^{(1,1)^*}$ is an effective, reduced collision integral,

$$\Omega_{avg}^{(1,1)^*}=\frac{\Omega_D^{(1,1)^*}+\mathrm{Kn}\left(0.9\Omega_D^{(1,1)^*}+0.1\Omega_S^{(1,1)^*}\right)-\frac{0.9\mathrm{Kn}\left(\Omega_D^{(1,1)^*}-\Omega_S^{(1,1)^*}\right)}{\left[1+(r/2.5\times10^{-9})^{15}\right]}}{1+\mathrm{Kn}} \tag{13}$$

$\Omega_D^{(1,1)^*}$, $\Omega_S^{(1,1)^*}$ are the reduced collision integrals for diffuse and specular scattering expressed by,

$$\begin{aligned}\Omega_D^{(1,1)^*}=&1+\frac{\pi}{8}+\left[1.072+\frac{2.078}{T^{*1/4}}+\frac{1.261}{T^{*1/2}}\right]\left(\frac{\sigma}{r}\right)\\&+\left[3.285-\frac{8.872}{T^{*1/4}}+\frac{5.225}{T^{*1/2}}\right]\left(\frac{\sigma}{r}\right)^2\end{aligned} \tag{14}$$

$$\begin{aligned}\Omega_S^{(1,1)^*}=&1+\left[0.316+\frac{1.47}{T^{*1/4}}+\frac{0.476}{T^{*1/2}}\right]\left(\frac{\sigma}{r}\right)\\&+\left[1.53-\frac{5.013}{T^{*1/4}}+\frac{4.025}{T^{*1/2}}\right]\left(\frac{\sigma}{r}\right)^2\end{aligned} \tag{15}$$

where T^* is the modified reduced temperature,

$$T^*=\frac{3k_B T}{2}\frac{m}{\pi\varepsilon\sigma^3\rho_l} \tag{16}$$

and $\sigma=(\sigma_g+\sigma_d)/2$, $\varepsilon=\sqrt{\varepsilon_g\varepsilon_d}$, where σ are the self-collision diameter, ε the well depth of the Lennard-Jones potential function for the constituent atom or molecule, m the mean atomic mass of the droplet.

Without solving the energy equation of the liquid phase, the droplet temperature can be determined by an explicit model [12]. The explicit model is deduce from the energy conservation for the droplet by using the quasi-steady "wet-bulb approximation", and the high accuracy is proved in the whole range of relevant growth [33].

$$\left(\frac{T_d}{T_\infty}-1\right)=f(S_\infty-\mathrm{Ke}_\infty)[C_1+C_2]^{-1}(1-\delta_1) \tag{17}$$

where

$$\mathrm{Ke}=\frac{2\sigma_p}{\rho_l R_v T_d r} \tag{18}$$

$$\delta_1=\frac{\frac{1}{2}C_1^2-C_2}{(C_1+C_2)^2}(\ln S_\infty-\mathrm{Ke}_\infty) \tag{19}$$

$$f(S_\infty,\mathrm{Ke}_\infty)=\ln S_\infty-\mathrm{Ke}_\infty \tag{20}$$

$$C_1=\frac{T_\infty}{\theta_\infty S_\infty}\left(\frac{p_\infty}{p_{s\infty}}-S_\infty\right) \tag{21}$$

$$C_2=\frac{h_{fg\infty}}{R_v T_\infty} \tag{22}$$

$$\theta_\infty=\left(\frac{D_{mod}}{k}\frac{\mathrm{Nu}_M^{tr}}{\mathrm{Nu}_E^{tr}}\right)_\infty \tag{23}$$

$$D_{mod}=\frac{D_m p}{R_v T_m} \tag{24}$$

$$T_m=\frac{1}{3}(2T_d+T_\infty) \tag{25}$$

where T_d stands for the droplet temperature, the subscript ∞ refers to the far field region, subscript m denotes that the physical properties are calculated at an intermediate temperature T_m. Ke is

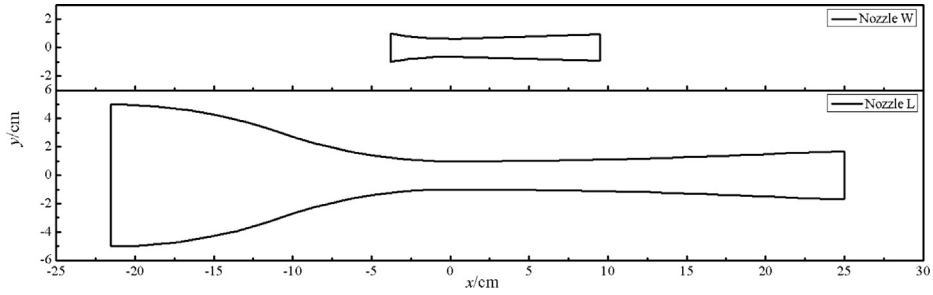

Fig. 2. Geometrical structures of the supersonic nozzles.

the Kelvin factor, S the supersaturation ratio, σ_p the surface tension, and D_{mod} is the modified diffusion coefficient.

2.2. No-slip model

In the absence of velocity slip, it is assumed that the two phases have the same averaged velocity, thus the flow can be described by a homogeneous two-phase model. The gas conservation equations of mass, momentum and energy are,

$$\frac{\partial \rho_g}{\partial t} + \frac{\partial}{\partial x_j}\left(\rho_g u_j\right) = 0 \tag{26}$$

$$\frac{\partial\left(\rho_g u_i\right)}{\partial t} + \frac{\partial}{\partial x_j}\left(\rho_g u_j u_i\right) = -\frac{\partial p}{\partial x_i} + \frac{\partial \tau_{ij}}{\partial x_j} \tag{27}$$

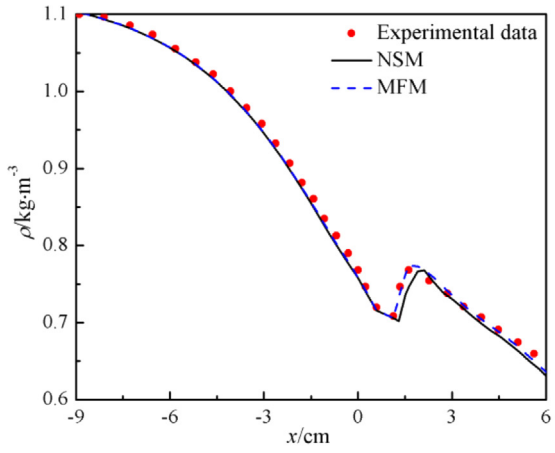

(a) Centerline density distribution of nozzle L

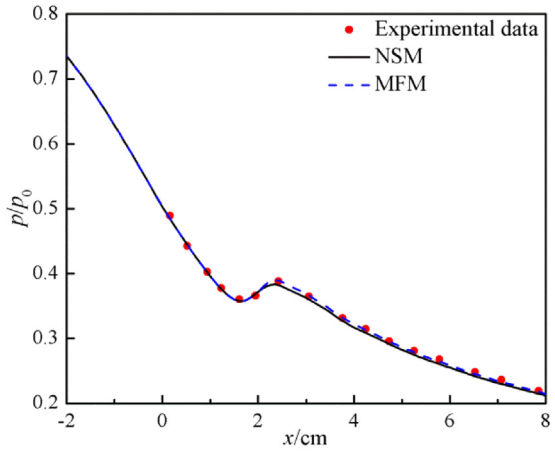

(b) Centerline pressure ratio distribution of nozzle W

Fig. 3. Comparisons between the predicted results of proposed models and experimental data.

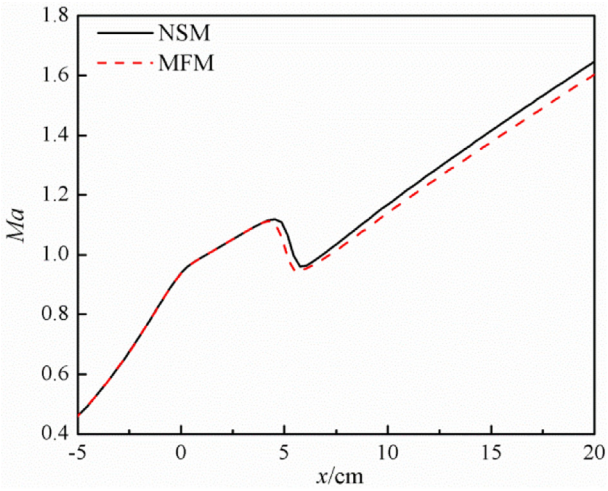

(a) Nozzle L

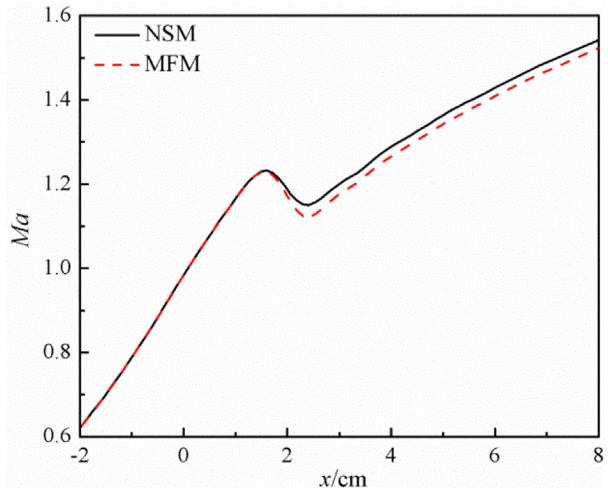

(b) Nozzle W

Fig. 4. Gas Mach number along the nozzle centerline.

$$\frac{\partial \rho_g E_g}{\partial t} + \frac{\partial}{\partial x_j}\left(u_j\left(\rho_g E_g + p\right)\right) = -\frac{\partial q_j}{\partial x_j} + \frac{\partial\left(u_i \tau_{ij}\right)}{\partial x_j} + \beta \dot{m} h_{fg} \tag{28}$$

Since the two phases share the same velocity, the momentum equations of liquid phase can be ignored. The transport equations of liquid phase also follow Hill's method shown in Equations (4)–(7), which are almost identical with that of the multi-fluid model except the momentum equations. The calculations of droplet temperature follow the explicit model shown in Equations (17)–(25).

2.3. Nucleation and droplet growth model

Accounting for the effects of carrier gas, the nucleation rate is calculated by the internally consistent classical theory (ICCT) [34],

$$J = KS \exp\left(\theta - \frac{4}{27}\frac{\theta^3}{(\ln S)^2}\right) \tag{29}$$

where the prefactor K and the dimensionless surface tension can be calculated as follows:

$$K = \left(\frac{p_s f_e}{Z_g k_B T}\right)^2 \left(\frac{2\sigma_p m}{\pi}\right)^{1/2} \frac{1}{\rho_l} \tag{30}$$

$$\theta = (36\pi)^{1/3} \left(\frac{m}{\rho_l}\right)^{2/3} \frac{\sigma_p}{k_B T} \tag{31}$$

where Z_g is the compressibility of the gas, p_s is the saturation vapor pressure, σ_p the pressure-dependent surface tension. The presence of the carrier gas will affect the vapor equilibrium fugacity [35], and the increase of equilibrium fugacity with the saturated vapor pressure is referred to as enhancement factor f_e. Correlation of enhancement factor for water–nitrogen mixture used in the following text can be expressed by [36],

$$\ln(f_e) = b(T) \times [p - p_s(T)] \tag{32}$$

$$b(T) = 4.42 \times 10^{-2} - 3.03 \times 10^{-4} T + 7.31 \times 10^{-7} T^2 - 5.98 \times 10^{-10} T^3 \tag{33}$$

To estimate the effect of carrier gas adsorption on nucleation, the pressure-dependent surface tension is used [5],

$$\sigma_p = \sigma_0 - n_a k_B T \ln\left(\frac{p + p_L}{p_L}\right) \tag{34}$$

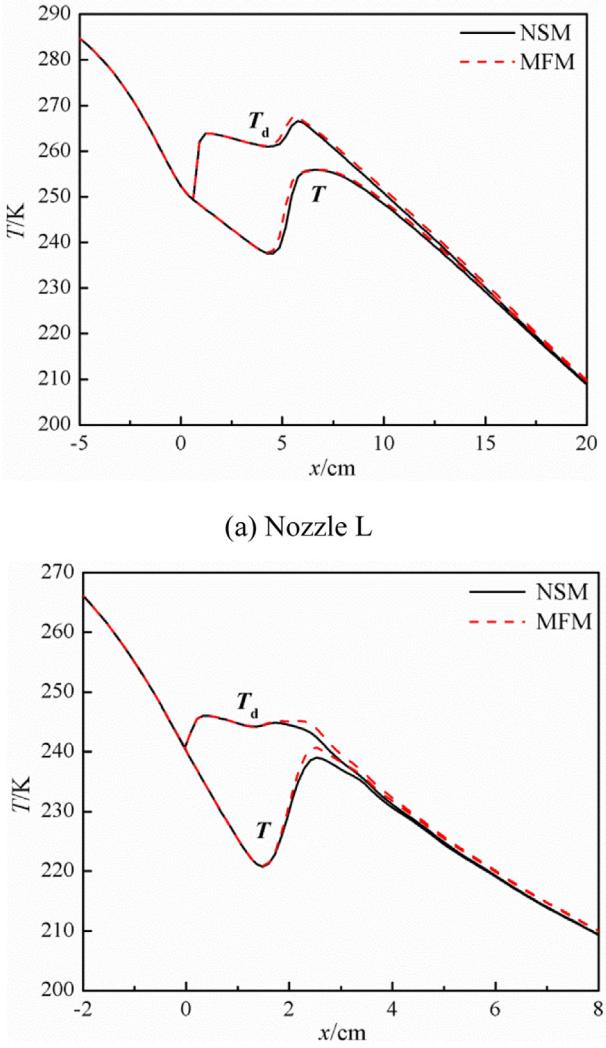

Fig. 5. Gas and droplet temperature along the nozzle centerline.

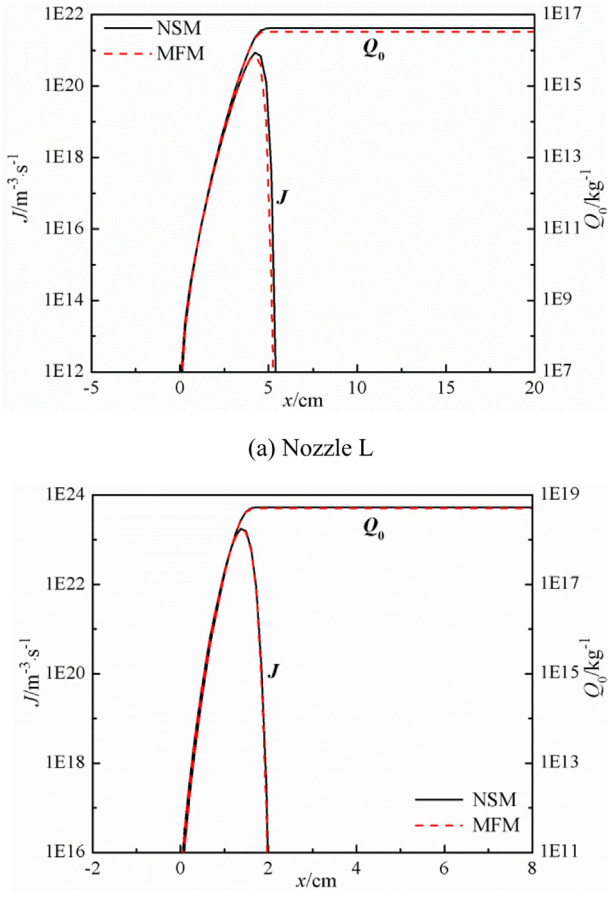

Fig. 6. Nucleation rate and droplet number density along the nozzle centerline.

where σ_0 is surface tension of the pure liquid, n_a is the number of adsorption sites per unit area, approximately 6×10^{18} m^{-2}, and p_L is the Langmuir reference pressure.

The Gyarmathy model [12] is adopted to calculate the droplet growth rate, which gives a better description of the droplet growth for a variety of binary mixtures [37].

$$\frac{dr^2}{dt} = -\frac{Nu_M^{tr} D_{mod}}{\rho_l} \frac{p_{v\infty} - p_v^{eq}}{p_{g\infty}} \tag{35}$$

where Nu_M^{tr} is Nusselt number for mass transfer in transition regime, p_v^{eq} is the equilibrium vapor pressure. $p_{v\infty}$ and $p_{g\infty}$ are partial pressure of the vapor and carrier gas in far field region, respectively. More details can be found elsewhere [23].

2.4. Numerical implementations

The simulations are implemented using the ANSYS-FLUENT software. The finite-volume method and second order upwind scheme are employed to discretize the conservation equations. The density-based solver is adopted for the gas equations, and the liquid phase transport equations are added by the introduction of User-Defined Scalars (UDS). The phase-change models, the source terms, turbulent diffusion term and other terms abovementioned are embedded through User-Defined Functions (UDF). Besides, structured grids are adopted and refined in the rapidly changing nucleation region. As to the boundary conditions, total pressure and temperature are imposed at the inlet boundary, and the UDS are set to zero, with supersonic outflow as the outlet conditions. The no-slip condition is used at the solid wall. The solution is converged to normalized RMS residuals of the order of 10^{-5} or lower for all transport equations in this paper.

3. Model validations

The experimental data for the condensing flow in transonic nozzles conducted by Wyslouzil et al. [11] (denoted as nozzle W) and Lamanna et al. [22] (denoted as nozzle L) have been used to validate the proposed models. The geometrical sizes of the two nozzles are shown in Fig. 2, where the nozzle throat is located at $x = 0$. The nozzle W has a diverging section with the length of 9.5 cm, and the divergence angle is 1.8°in the linear region. The length of diverging section of nozzle L is 25 cm, and the divergence angle is approximately 3° near the nozzle exit, while the divergence angle is very small before the location $x = 5$ cm, less than 1.0°. The humid nitrogen is

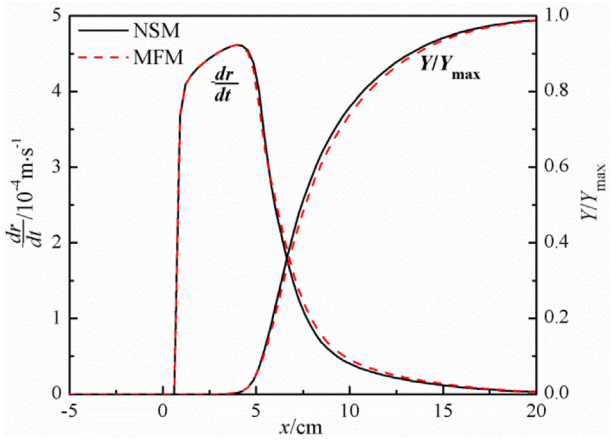

(a) Nozzle L

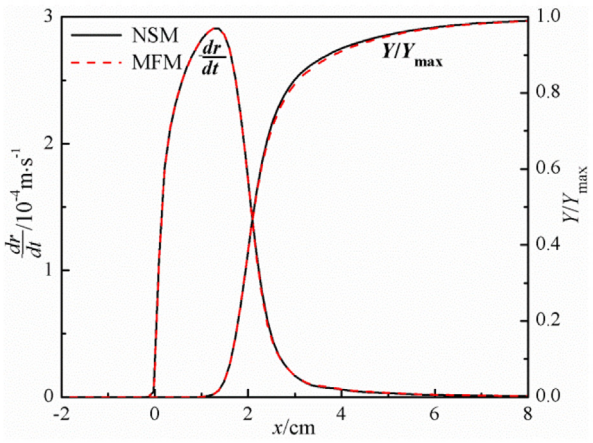

(b) Nozzle W

Fig. 7. Droplet growth rate and wetness fraction along the nozzle centerline.

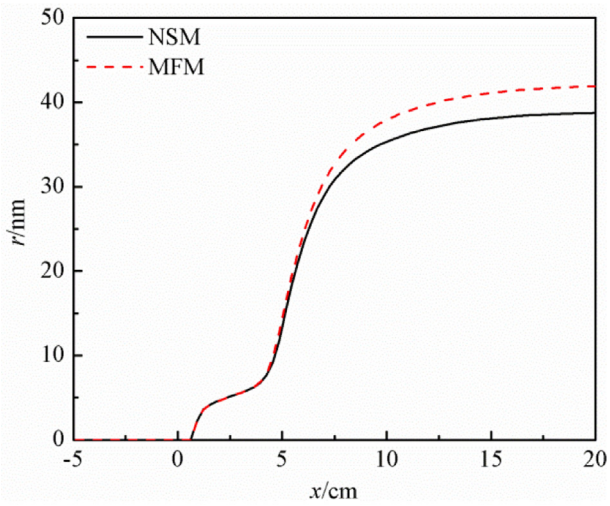

(a) Nozzle L

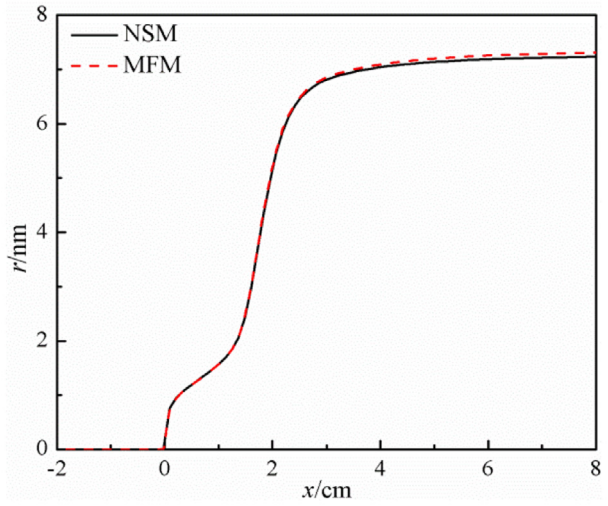

(b) Nozzle W

Fig. 8. Droplet radius along the nozzle centerline.

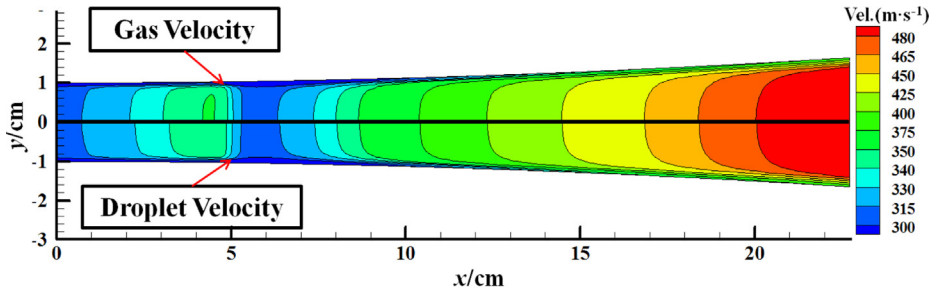

(a) Nozzle L

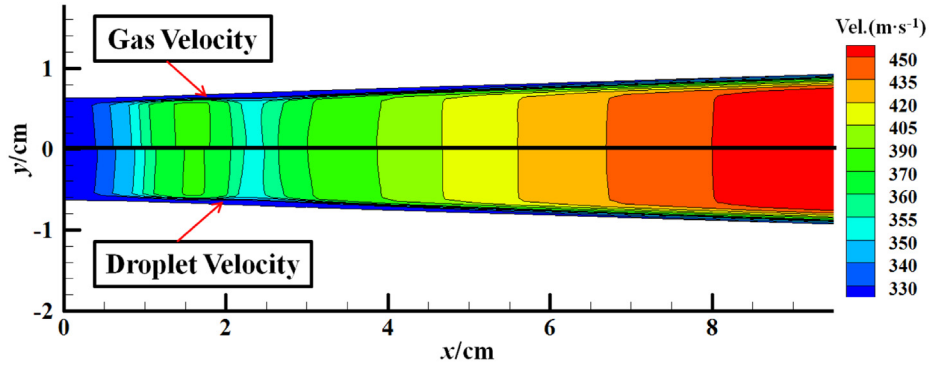

(b) Nozzle W

Fig. 9. Contours of gas and liquid velocity predicted by the multi-fluid model.

used as the working gas in both experiments. The inlet conditions of nozzle W are the total pressure 0.6 bar, the total temperature 286.7 K, and the vapor partial pressure 0.01 bar, while inlet conditions of nozzle L are the total pressure 0.913 bar, the total temperature 283.1 K, and the stagnation supersaturation ratio 0.613, with supersonic outflow conditions for both cases. For comparison, both multi-fluid model (MFM) and no-slip model (NSM) are tested. Fig. 3 compares the predicted results obtained from the two models against the experimental data along the nozzle axis.

As shown in Fig. 3, the simulated results of both models agree well with the experimental data. It is apparently seen that multi-fluid model shows a better performance than the no-slip model. In the multi-fluid model, the predicted results of the location and intensity of the condensation shock agree better with the experimental data, while the intensity of the condensation shock is underestimated by the no-slip model. The analysis above indicates that the multi-fluid model proposed in this paper shows good accuracy in the prediction of condensing flow in the presence of carrier gas.

4. Results and discussion

In order to demonstrate the typical fluid dynamic behavior and the droplet condensation characteristics, the predictions of non-equilibrium condensing flow in the above two nozzles are undertaken. The inlet conditions of nozzle W are total pressure 0.6 bar, total temperature 286.7 K, and vapor partial pressure 0.01 bar, while the inlet conditions of nozzle L are total pressure 0.867 bar, total temperature 296.6 K, and the stagnation supersaturation ratio 0.5.

4.1. Physical description of non-equilibrium condensation

The variation in the fluid dynamic parameters such as Mach number, gas and droplet temperature, together with the condensation parameters such as nucleation rate, droplet number density, droplet growth rate, wetness fraction and droplet radius along the nozzle axis are shown in Figs.4–8, respectively. From these results, the important physical features of the condensation process in supersonic nozzles have been captured. The continuing expansion of the gas mixture in the transonic nozzles results in reduction of pressure and temperature, which give rises to the nucleation of the condensable vapor. The onset of nucleation can be observed from the steep rise in the nucleation rate and droplet number density shown in Fig. 6, while no perturbation of the flow properties is observed. Once the droplet growth process starts, the liquid mass fraction and droplet size increase (seen in Figs. 7 and 8), and a large amount of latent heat is released to the flow inducing a condensation shock. When the condensation shock emerges, the pressure, temperature and density significantly rise, and also the Mach number decreases, as shown in Figs. 3–5.

4.2. Effects of inter-phase slip

It should be noted that some differences arise between the numerical results of the two models due to the effects of inter-phase slip. For the multi-fluid model, there is no doubt that the negative inter-phase drag force exerted on the gas phase lowers the gas velocity in the gas-droplet flow comparing with the no-slip flow, as seen in Fig. 4. Comparing the predicted results of the two models, a relatively high pressure, density and temperature is obtained as the consequence of relatively low gas velocity predicted in the multi-fluid model, shown in Figs. 3 and 5. It is clear that the inter-phase slip also affects the condensation parameters. As can be seen from Fig. 6, the nucleation rate and droplet number density predicted by the multi-fluid model is a little smaller than that predicted by the no-slip model, which is attributed to the lower supersaturation caused by increase of gas pressure and temperature. Subsequently, the lower droplet number density results in a

higher droplet growth rate and larger mean droplet radius, observed in Figs. 7 and 8. Owing to the low number density, the droplet wetness fraction predicted by the multi-fluid model is a little lower than the no-slip model during the earlier stage of condensation, but the difference tends to be smaller as the droplets grow, as seen in Fig. 7. Near the exit of the nozzles, both predicted wetness fraction are almost equal to 1.0, which indicates that all condensable vapor has already condensed into droplets in the sufficiently long divergent section.

Comparing the predictions in nozzles L and W, the effects of inter-phase slip with different expansion rate have been analyzed. The nozzle W has a shorter divergence section with a higher expansion rate, while the nozzle L has a very low expansion rate before the location $x = 5$ cm and a higher expansion rate near the nozzle exit. In nozzle W, compared with the results predicted by the two models, the effects of inter-phase slip on the condensation parameters are minor, but the effects on the flow parameters are noteworthy. Relatively, effects of inter-phase slip in nozzle L are significant for all parameters. It is well known that the inter-phase velocity slip mainly depends upon the droplet size and the flow properties of the two-phase flow. Due to the high expansion rate in nozzle W, a rapid condensation occurs in a very short distance, resulting in formation of small-size droplets, thus there is almost no velocity slip at the initial stage of condensation, and obvious inter-phase slip is observed until the droplets grow to a certain size. Therefore, the inter-phase slip almost has no influence on the condensation parameters, while it affects the flow parameters significantly once the droplets size is large enough. In nozzle L, the generated droplets are large enough to induce the inter-phase slip during most of the condensation process, owing to its low expansion rate. Consequently, both the condensation parameters and the flow parameters are affected in the whole process.

From these results, it is concluded that the effects of inter-phase slip should not be neglected in the condensing flow, especially in the case of low expansion rate, which is clarified by the newly developed multi-fluid model.

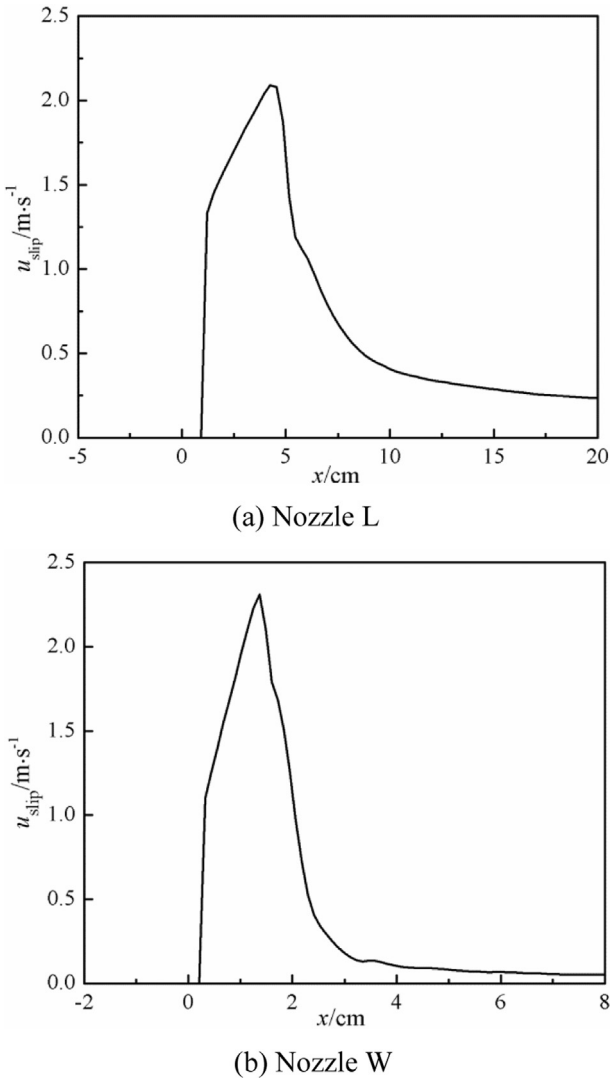

Fig. 10. Distribution of slip velocity along the nozzle centerline.

4.3. Two-phase thermal non-equilibrium

Fig. 5 illustrates the gas and droplet temperature along the nozzle centerline. It is observed that large temperature difference exists between the gas and liquid droplet at the initial stage of condensation, but the inter-phase temperature difference tends to vanish at the end of condensation process. At the initial stage of the condensation, the inter-phase temperature difference appears at a high value, while heat can be conducted from the droplet surface to the surrounding gas. Meanwhile, the vapor is in highly supercooled state, leading to the formation of substantive condensation nuclei. The release of the condensation latent heat is not enough to perturb the flow parameters at the initial stage of condensation, thus the gas temperature still decreases rapidly due to the expansion. However, the droplet temperature does not decrease significantly due to the latent heat liberation to the liquid phase. As the droplets grow, the mass fraction and size of the droplets increase accompanying with amounts of latent heat released, thereby making a sharp increase of gas temperature at where the condensation shock is formed. Meanwhile, the droplet temperature rises, and the inter-phase temperature difference dramatically decreases. After the condensation shock, the gas temperature decreases, and the droplets are effectively cooled down by the high concentration carrier gas in the absence of the latent heat. At the end of condensation process, the gas and droplet temperatures relax to near equilibrium value, and the inter-phase temperature difference almost disappears.

4.4. Two-phase inertial non-equilibrium

Fig. 9 shows the two-phase velocity predicted by the multi-fluid model in the divergent section of the nozzles L and W. The upper half of this figure is the distribution of the gas phase velocity, and the bottom half is the distribution of the liquid phase velocity. As seen in the figure, apparent velocity differences are observed near the location of the condensation shock, while the gas and liquid velocities are almost the same in the downstream of the shock. Fig. 10 presents the quantitative distribution of the slip velocity along the nozzle centerline. It's observed that the slip velocity suddenly increases to a relative maximum value (1–2 m/s) in a very short distance, followed by a slow decrease until the equilibrium is reached. In this study, the forces imposed on the gas phase generally include the pressure difference and an inter-phase drag force, of which the pressure difference is the primary factor that leads to the change of gas phase velocity. The forces acting on the droplet is the same as the gas phase except that the inter-phase drag force is in the opposite direction. Since the liquid density is far greater than the gas density, the influence of the pressure difference on the liquid droplet can be easily ignored comparing with the gas phase, and the droplet motion is mainly driven by the momentum of the gas molecules condensed on the droplet and the

drag force. At the initial stage of condensation, the sudden generation of liquid droplets gives rise to a large slip velocity in a very short distance due to the inertia. As the condensation shock emerges, the gas phase velocity has an abrupt decrease, however, due to the inertial effect, the slow response of liquid-phase make it take a longer distance to adjust its velocity to the gas flow, hence the inter-phase slip velocity decreases. In the effect of inter-phase drag force, the inter-phase slip velocity continues to decrease after the condensation shock until the two-phase velocity equilibrium is established. Ultimately, the inter-phase velocity slip almost disappears and maintains unless new flow perturbations emerge.

5. Conclusions

A mathematical multi-fluid model has been developed to study the condensing flow in the presence of carrier gas. Different from the traditional no-slip model, this newly developed model considers both the inter-phase velocity slip and temperature difference between two phases. It is able to reflect the two-phase thermal and inertial non-equilibrium in the condensing flow. To determine the effects of inter-phase slip, the numerical simulations of condensing flow have been conducted in transonic nozzles by employing the proposed multi-fluid model and the no-slip model for comparison. The multi-fluid model is found to agree better with the experimental data available. The results show that even though the velocity slip (1–2 m/s) is much smaller than the bulk velocity (400–500 m/s), the influence of the velocity slip on the flow parameters and condensation parameters is considerable, especially in the case of low expansion rate. The velocity slip and temperature difference are significant at the initial stage of condensation. Once the gas–liquid equilibrium reaches, the inter-phase slip and temperature difference fade out.

Acknowledgements

The authors acknowledge two National Nature Science Foundations of China under the Contract Nos. 51276140 and 51121092 for financial support.

Nomenclature

b	correlation coefficient for enhancement factor
C_1	dimensionless parameter for calculation of droplet temperature
C_2	dimensionless parameter for calculation of droplet temperature
D	diffusion coefficient, kg m^{-1} s^{-1}
$\mathrm{d}\bar{r}/\mathrm{d}t$	droplet growth rate, m s^{-1}
E	total energy, J kg^{-1}
f_e	enhancement factor
$\boldsymbol{F_D}$	inter-phase drag force, N m^{-3}
h_{fg}	latent heat, J kg^{-1}
J	nucleation rate, m^{-3} s^{-1}
k	thermal conductivity, W m^{-1} K^{-1}
K	prefactor for calculating nucleation rate, m^{-3} s^{-1}
k_{B}	Boltzmann's constant ($=1.3807 \times 10^{-23}$ J K^{-1})
Ke	Kelvin number
Kn	Knudsen number
m	mass, kg
$\dot{m}$	mass condensation rate, kg m^{-3} s^{-1}
n_{a}	number of adsorption sites per unit area, m^{-2}
N	number density of the gas, m^{-3}
Nu	Nusselt number
p	pressure, Pa
p_{L}	Langmuir reference pressure, Pa
q	conductive heat flux, W m^{-2}
Q_0	zeroth moment of the droplet size distribution, kg^{-1}
Q_1	first moment of the droplet size distribution, m kg^{-1}
Q_2	second moment of the droplet size distribution, m^2 kg^{-1}
r	droplet radius, m
R	gas constant, J mol^{-1} K^{-1}
S	supersaturation ratio
T	temperature, K
T^*	modified reduced temperature
u	velocity, m s^{-1}
$\boldsymbol{V}$	relative velocity, m s^{-1}
x	spatial dimension, m
Y	mass fraction of liquid droplets, kg kg^{-1}
Z_g	gas compressibility

Greek symbols

α	volume fraction
β	proportion of the latent heat absorbed by the carrier gas
δ_1	correction factor for calculation of droplet temperature
ε	Lennard-Jones well depth, J
θ	dimensionless surface tension
θ_∞	parameter for calculation of droplet temperature, K
μ	viscosity, kg m^{-1} s^{-1}
ρ	density, kg·m^{-3}
σ_{p}	pressure-dependent surface tension, N m^{-1}
σ	Lennard-Jones collision diameter, m
σ_0	surface tension of the pure liquid, N m^{-1}
σ_{t}	turbulent Prandtl number
τ	shear stress, N m^{-2}
Γ_{t}	turbulent diffusivity, kg m^{-1} s^{-1}
Ω	reduced collision integral

Superscripts

$-$	mean
eq	equilibrium state
tr	transition regime
(1,1)*	reduced collision integral of diffusivity

Subscripts

avg	average scattering
c	critical state
d	droplet
D	diffuse scattering
$\dot{E}$	energy transfer
f	fluid
g	gas
ij	tensor notation
l	liquid
m	intermediate state
mod	modified
$\dot{M}$	mass transfer
r	reduced
S	specular scattering
s	saturated state
t	turbulent
v	vapor
∞	far field region

References

[1] B. Prast, P. Schinkelshoek, B. Lammers, M. Betting, CFD for supersonic gas processing, in: NEL Multiphase Separation and Multiphase Pumping Technologies Conference, September 1–2, 2005, pp. 53–58. Aberdeen, UK.
[2] D. Labetski, Nucleation of *n*-nonane in Mixtures of Methane, Propane, and Carbon Dioxide, Technische Universiteit Eindhoven, The Netherlands, 2007.

[3] N.M. Kortsenshteyn, A.K. Yastrebov, Interphase heat transfer during bulk condensation in the flow of vapor–gas mixture, Int. J. Heat Mass Transfer 55 (2012) 1133–1140.
[4] S. Hamidi, M. Kermani, Numerical solution of compressible two-phase moist-air flow with shocks, Eur. J. Mech. B-Fluids 42 (2013) 20–29.
[5] C. Luijten, M. Van Dongen, Nucleation at high pressure. I. Theoretical considerations, J. Chem. Phys. 111 (1999) 8524–8534.
[6] A.S. Bhabhe, Experimental Study of Condensation and Freezing in a Supersonic Nozzle, The Ohio State University, USA, 2012.
[7] B. Somnath Sinha, Experimental and Modeling Study of Condensation in Supersonic Nozzles, The Ohio State University, USA, 2008.
[8] M. Anisimov, E. Fominykh, S. Akimov, P. Hopke, Vapor–gas/liquid nucleation experiments: a review of the challenges, J. Aerosol Sci. 40 (2009) 733–746.
[9] G. Lamanna, J. van Poppel, M. van Dongen, Experimental determination of droplet size and density field in condensing flows, Exp. Fluids 32 (2002) 381–395.
[10] R. Heist, H. He, Review of vapor to liquid homogeneous nucleation experiments from 1968 to 1992, J. Phys. Chem. Ref. Data 23 (1994) 781–806.
[11] B. Wyslouzil, C. Heath, J. Cheung, G. Wilemski, Binary condensation in a supersonic nozzle, J. Chem. Phys. 113 (2000) 7317.
[12] G. Gyarmathy, The Spherical Droplet in Gaseous Carrier Streams: Review and Synthesis, in: Multiphase Science and Technology, Springer Verlag, Berlin, 1982.
[13] J. Young, The condensation and evaporation of liquid droplets at arbitrary Knudsen number in the presence of an inert gas, Int. J. Heat Mass Transfer 36 (1993) 2941–2956.
[14] G. Schnerr, U. Dohrmann, Transonic flow around airfoils with relaxation and energy supply by homogeneous condensation, AIAA J. 28 (1990) 1187–1193.
[15] D. Simpson, A. White, Viscous and unsteady flow calculations of condensing steam in nozzles, Int. J. Heat Fluid Flow 26 (2005) 71–79.
[16] R. Kumar, Z. Li, D.A. Levin, Modeling of carbon dioxide condensation in the high pressure flows using the statistical BGK approach, Phys. Fluids 23 (2011) 052001.1–052001.15.
[17] C. Delale, M. Muitjens, M. Van Dongen, Asymptotic solution and numerical simulation of homogeneous condensation in expansion cloud chambers, J. Chem. Phys. 105 (1996) 8804–8821.
[18] A.G. Gerber, Two-phase Eulerian/Lagrangian model for nucleating steam flow, J. Fluids Eng. 124 (2002) 465–475.
[19] M. Kermani, A. Gerber, A general formula for the evaluation of thermodynamic and aerodynamic losses in nucleating steam flow, Int. J. Heat Mass Transfer 46 (2003) 3265–3278.
[20] R. Jansen, A Lagrangian–Eulerian approach to modeling homogeneous condensation in high density gas expansions, J. Chem. Phys. 134 (2011) 104105.
[21] A. Gerber, M. Kermani, A pressure based Eulerian–Eulerian multi-phase model for non-equilibrium condensation in transonic steam flow, Int. J. Heat Mass Transfer 47 (2004) 2217–2231.
[22] G. Lamanna, On Nucleation and Droplet Growth in Condensing Nozzle Flows, Technische Universiteit Eindhoven, Eindhoven, 2000.
[23] X. Luo, B. Prast, M. Van Dongen, H. Hoeijmakers, J. Yang, On phase transition in compressible flows: modelling and validation, J. Fluid Mech. 548 (2006) 403–430.
[24] S. Dykas, W. Wróblewski, Single- and two-fluid models for steam condensing flow modeling, Int. J. Multiphase Flow 37 (2011) 1245–1253.
[25] X. Wu, L. Li, G. Li, Z. Feng, Numerical simulation of wet steam condensing flow based on a two-fluid model, in: International Conference on Power Engineering, 2007, October 23–27, pp. 1331–1336. Hangzhou, China.
[26] A.G. Gerber, Inhomogeneous multifluid model for prediction of nonequilibrium phase transition and droplet dynamics, J. Fluids Eng. 130 (2008) 031402.
[27] S. Dykas, W. Wróblewski, Two-fluid model for prediction of wet steam transonic flow, Int. J. Heat Mass Transfer 60 (2013) 88–94.
[28] I. Jones, P. Guilbert, M. Owens, I. Hamill, C. Montavon, J. Penrose, B. Prast, The use of coupled solvers for complex multi-phase and reacting flows, in: Proceedings of the Third International Conference on CFD in the Minerals and Process Industries, 2003, December 10–12, pp. 13–20. Melbourne, Australia.
[29] ANSYS FLUENT, Theory Guide (Release 14.0), in: Multiphase Flows, ANSYS, Inc., November 2011, pp. 491–616 (Chapter 17).
[30] S.L. Soo, Fluid Dynamics of Multiphase Systems, Blaisdell Publishing Company, Waltham, 1967.
[31] P.G. Hill, Condensation of water vapour during supersonic expansion in nozzles, J. Fluid Mech. 25 (1966) 593–620.
[32] Z. Li, H. Wang, Drag force, diffusion coefficient, and electric mobility of small particles. II. Application, Phys. Rev. E 68 (2003) 061207.1–061207.13.
[33] H.J. Smolders, Non-linear Wave Phenomena in a Gas–Vapor Mixture with Phase Transition, Eindhoven University of Technology, The Netherlands, 1992.
[34] P. Peeters, J. Hrubý, M.E.H. van Dongen, High pressure nucleation experiments in binary and ternary mixtures, J. Phys. Chem. B 105 (2001) 11763–11771.
[35] J.A. Fisk, J.L. Katz, Condensation of supersaturated vapors. X. Pressure and nonideal gas effects, J. Chem. Phys. 104 (1996) 8649–8656.
[36] C. Luijten, K. Bosschaart, M. Van Dongen, High pressure nucleation in water/nitrogen systems, J. Chem. Phys. 106 (1997) 8116–8123.
[37] P. Peeters, C. Luijten, M. Van Dongen, Transitional droplet growth and diffusion coefficients, Int. J. Heat Mass Transfer 44 (2001) 181–193.